Substrate-Friendly Growth of Large-Sized $Ni(OH)_2$ Nanosheets for Flexible Electrochromic Films

*Liangliang Zhu, Wei Li Ong, Xin Lu, Kaiyang Zeng, Hong Jin Fan, and Ghim Wei Ho**

***L**arge-area, 2D, anisotropic, direct growth of nanostructures is considered an effective and straightforward way to readily fulfill transparent, flexible technology requirements. In addition, formation of thin hybrid structures by combining with another 2D material brings about dimensional advantages, such as intimate heterostructure functionalities, large specific area, and optical transparency. Here, we demonstrate 2D planar growth of thin $Ni(OH)_2$ nanosheets on arbitrary rigid and soft supports, by exploiting the growth strategies of oriented attachment induced by interfacial chemistry and the intrinsic driving force of layered structure constitution. Moreover, large-scale 2D heterohybrids have successfully been prepared by direct conformal growth of $Ni(OH)_2$ nanosheets overlying MoO_3 nanobelts. Unlike the exfoliation and transfer of 2D materials technique, this approach minimizes multiple process contamination and physical-handling structural defects. Accordingly, proof-of-concept flexible electrochromism is demonstrated in view of its prerequisite to the access of a large homogeneous material coating. The as-synthesized 2D layered structure affirms its optical and electrochemical superiority through the display of wide optical modulation, high coloration efficiency, good cyclic stability, and flexibility.*

2D nanosheets are thin, layered, crystalline solids with the defining characteristics of intralayer covalent and van der Waals bonding.[1] It is well known that other than material composition, lateral dimension, arrangement, and thickness of nanosheets play crucial roles in determining their fundamental properties.[2,3] In particular, thin and lamellarly arranged 2D nanosheets have recently garnered immense interest for both conventional electronics technology[4–6] and nascent flexible technology[7] because, amongst other considerations, these thin nanosheets bear ultimate structural mechanics and integrity. Furthermore, the development of graphene and its methodology has expedited 2D nanosheets progress, which has particularly benefited flexible electronics because of their unrivaled mechanical virtues when deposited on soft polymeric or plastic substrates.[8] However, large-scale, cost-effective production methods, in parallel to ease of fabrication and materials quality, are the main challenges to fulfill an emerging era of 2D flexible technology.

Dr. L. L. Zhu, Dr. W. L. Ong, X. Lu, Prof. G. W. Ho
Department of Electrical and Computer Engineering
National University of Singapore
4 Engineering Drive 3, 117583, Singapore
E-mail: elehgw@nus.edu.sg

Prof. K. Y. Zeng
Department of Mechanical Engineering
National University of Singapore
9 Engineering Drive 1, 117576, Singapore

Prof. H. J. Fan
School of Physical and Mathematical Sciences
Nanyang Technological University
637371, Singapore

Prof. G. W. Ho
Engineering Science Programme
National University of Singapore
9 Engineering Drive 1, 117575, Singapore

Prof. G. W. Ho
Institute of Materials Research and Engineering
A*STAR (Agency for Science, Technology and Research)
3 Research Link, 117602, Singapore

DOI: 10.1002/smll.201700084

Besides single component nanosheets, heterohybrids composed of different layered materials that are stacked vertically have recently been perceived as a new avenue to actively tune desired 2D composite properties.[9–12] Notably, integration of planar heterohybrids into nanodevices could bring about phenomenal device physics to future technologies,[13] where ultrathin, transparent, efficient, and flexible capabilities are in demand. As such, preparing thin, transparent, and planar 2D heterohybrids on a large-scale is one of the major research endeavors. Already considerable processing efforts have especially been devoted to production, placement, and handling of the susceptible, thin, 2D layered materials. To date, various methods through dry mechanical and wet intercalation and/or direct sonication exfoliation have been developed to access thin 2D materials.[14–16] Dry exfoliation involves cleaving of layered materials into thin sheets by mechanical, electrostatic, or electromagnetic forces, while liquid exfoliation exploits sonication to extract thin layers, and generally engages multiple steps of material dispersion, exfoliation, and centrifugal purification.[16] The key challenge is to maintain large lateral dimensions of the exfoliated sheets, since multiple processing steps and sonication cause detrimental breaking up of the nanosheets. Albeit, a large-area, 2D, heterolayered, stacked nanodevice has been reported; it is meticulously built upon laborious and repetitive physical exfoliation and transfer of different layers.[17,18] Hence, obtaining uniform, outstretched 2D thin film sheets in large-scale and of high-quality, with minimal structural tearing, proves to be challenging with such an approach. In contrast, direct growth of 2D heterolayered semiconductors is proposed as an ideal straightforward method to abstain integrated 2D material systems from multiple process contamination and physical handling structural defect/tear.[19]

Herein, we demonstrate 2D anisotropic conformal growth of large-sized $Ni(OH)_2$ nanosheets on arbitrary rigid and soft substrates, as well as on MoO_3 nanobelts coated on substrate, to realize 2D heterohybrids on a large scale. In contrast, growth of 2D $Ni(OH)_2$ nanosheets on freestanding 2D MoO_3 nanobelts manifests in a 3D architecture of aggregated nanosheets that extends radially outward. The approach leverages on 2D oriented attachment induced by interfacial chemistry and the intrinsic driving force of layer structure formation that facilitates preparation of homogeneous planar 2D nanosheet film. Direct reactant adsorption on planar support acts as anchor sites for 2D oriented attachment and, as such, in situ interfacial interactions serve to guide conformal and lamellar growth of $Ni(OH)_2$ nanosheets. This solution-based approach exemplifies low-cost and scalable manufacturing, viable not only on rigid but also on soft platforms, leading to attractive mechanically-flexible attributes of bendable, rollable, and foldable structures. The combined structural advantages of thin conformal layered film and a 2D heterohybrid composition warrant high optical transparency, abundant electrochemical active sites, and structural stability. Accordingly, proof-of-concept electrochromism application is demonstrated, where large homogeneous 2D materials are requisite.[20–23] The as-synthesized 2D heterolayered hybrid of $Ni(OH)_2/MoO_3$ attests its optical and electrochemical superiority, which reveals wide optical modulation, high coloration efficiency, good cyclic stability, and flexibility.

Figure 1a shows top and cross-sectional schematics of direct growth of 2D $Ni(OH)_2$ film on a bare fluorine-doped tin oxide (FTO) substrate. A scanning electron microscopy

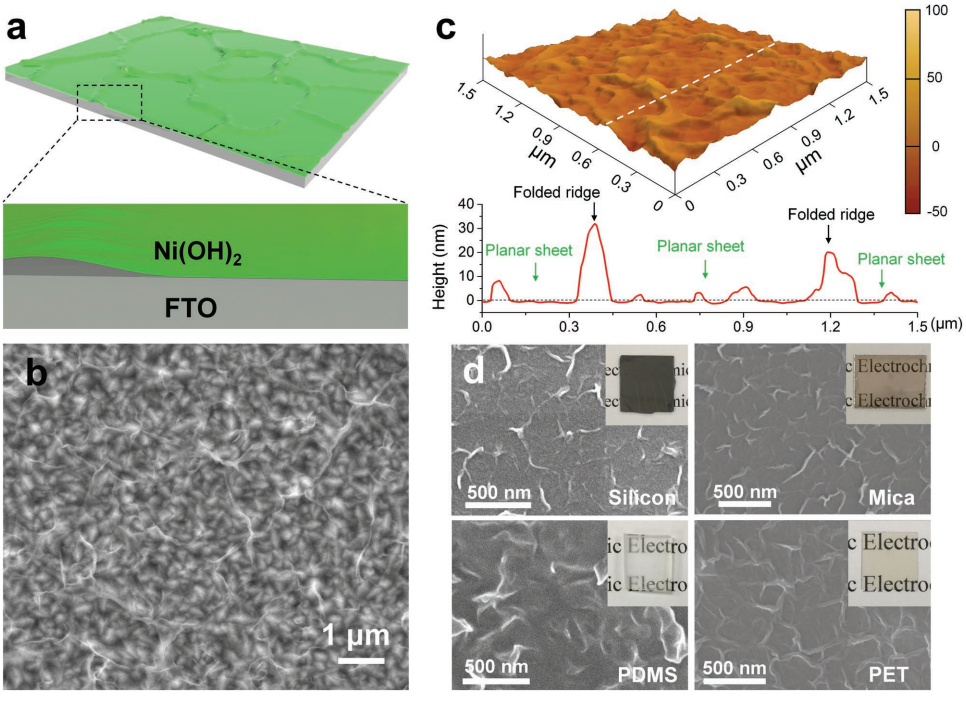

Figure 1. Growth of large-sized $Ni(OH)_2$ 2D sheets. a) Schematic illustrations of $Ni(OH)_2$ nanosheets grown on FTO and b) SEM image of the $Ni(OH)_2$/FTO. c) AFM 3D image of surface and height profiles along the white dash lines. d) SEM images of $Ni(OH)_2$ nanosheets grow on different substrate: silicon, mica, quartz, and PET. Insets are the corresponding digital photographs.

(SEM) image shows 2D anisotropic planar growth of layered $Ni(OH)_2$ nanosheets of ≈1–3 µm in lateral sizes, with folded edges on a large area (Figure 1b). The morphology and thickness of the $Ni(OH)_2$ nanosheets grown on FTO are also evaluated using tapping-mode atomic force microscopy (AFM), as shown in Figure 1c. The 3D AFM image indicates nanosheet morphology with the presence of surface corrugations. The topography and lateral dimension of these nanosheets are in good accordance with those seen in the SEM images. The variations in AFM height profile that is measured along the white dash line, display flat and ridge-like topography that correspond to the planar nanosheets and the folded overlapping edges. Furthermore, 2D anisotropic conformal growth of $Ni(OH)_2$ nanosheets are also attempted on various supports, namely silicon, mica, polydimethylsiloxane (PDMS), paper, and polyethylene terephthalate (PET) (Figure 1d). Collectively, 2D thin $Ni(OH)_2$ nanosheets can be demonstrated on both rigid and soft supports. The chemical compositions of FTO surface and $Ni(OH)_2$/FTO are also confirmed by fourier transform infrared (FTIR) spectra, as shown in **Figure 2**a. An obvious broad peak at 3250 cm^{-1} is ascribed to O—H, indicating the active surface, rich in hydroxyl groups. The bands appearing at regions between 3600–3000, 1700–1400, 1000–850, and 640 cm^{-1} can be assigned to the characteristic vibrations of O—H stretching, O—H bending, Ni—O stretching, and Ni—OH stretching.[24] The peaks at 1380 and 1305 cm^{-1} are due to the bending vibration of the residual NO^{3-} ions and stretching of C—N from hexamethylenetetramine (HMT).[25] On the basis of the aforementioned observations, a possible formation mechanism of 2D planar film is proposed and schematically presented in Figure 2b. As validated by FTIR analysis, the substrate surface is covered by abundant hydrophilic —OH groups, which provides rich nucleation sites for $Ni(OH)_2$ growth. Ni^{2+} precursor ions directly and homogeneously adsorbed onto the substrate surfaces covered with —OH group.[26–28] Consequently, planar nucleation sites lead to conformal growth of $Ni(OH)_2$ nanosheets on the substrate. The 2D anisotropic growth of $Ni(OH)_2$ is due to its intrinsic layered structure, which tends to crystallize into 2D lamellar materials, such as nanosheets or thin flakes. This approach exploits 2D oriented attachment, where direct reactant adsorption on planar support acts as anchor sites for in situ interfacial interactions that serve to guide conformal growth of $Ni(OH)_2$ nanosheets. The hydroxyl functional group cover on surface of PET, paper, mica, and PDMS, can be observed (Figure S1, Supporting Information). In contrast, quasi-continuous film of $Ni(OH)_2$ nanoparticles is observed on substrates (glass and quartz) that are deprived of hydroxyl group (Figure S2, Supporting Information). Experiments mentioned in the Supporting Information (Figure S3a–d) were carried out to affirm the —OH group on the substrates, which plays the key role in the conformal growth of $Ni(OH)_2$ nanosheets. These findings corroborate the proposed thin 2D planar growth that is facilitated by direct adsorption-oriented attachment and interfacial interaction with —OH rich surfaces under a constrained supply of growth precursor.

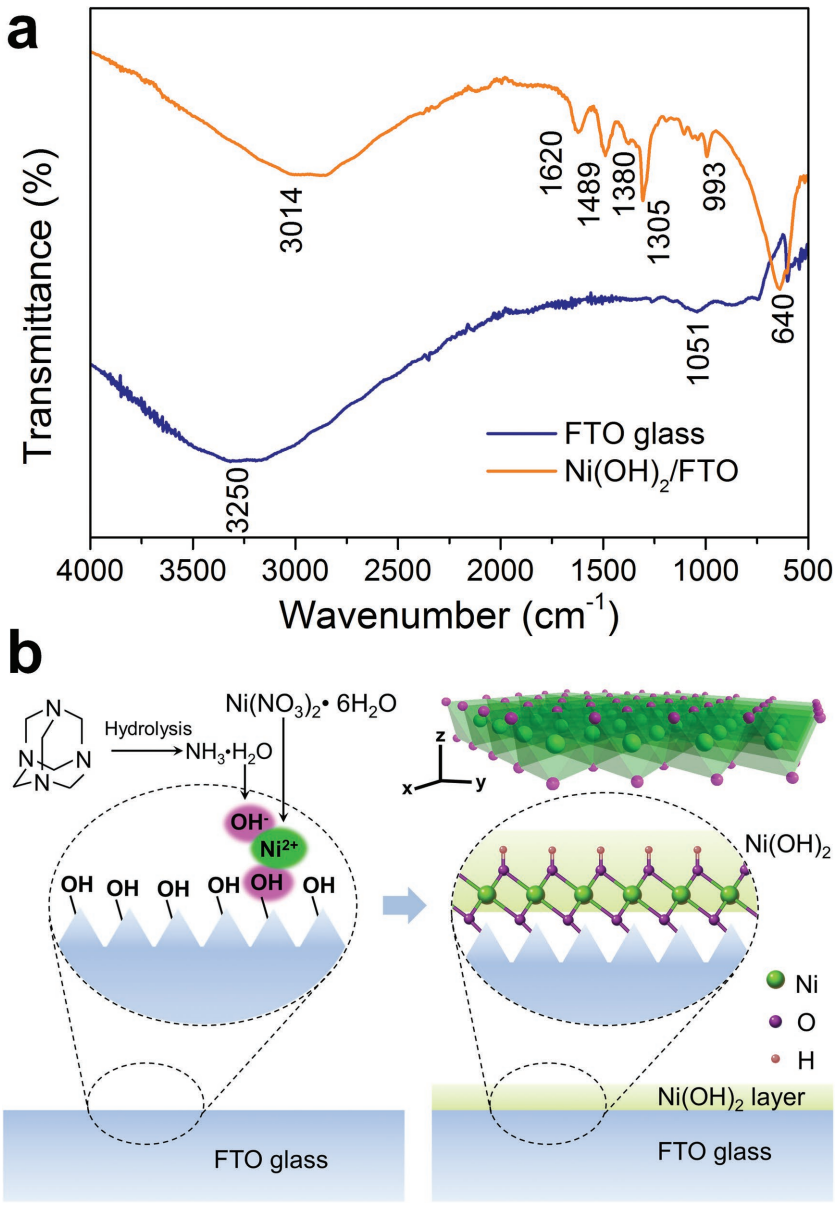

Figure 2. Mechanism of growth of large-sized $Ni(OH)_2$ 2D sheets. a) FTIR spectra of FTO glass and $Ni(OH)_2$/FTO. b) Schematic illustration of growth mechanism of large-sized $Ni(OH)_2$ 2D sheets.

To enhance the electrochromic performance, 2D heterohybrid is realized by first spray-coating preprepared MoO_3 nanobelts on an FTO substrate, followed by overlying growth of 2D $Ni(OH)_2$. **Figure 3**a shows the schematic

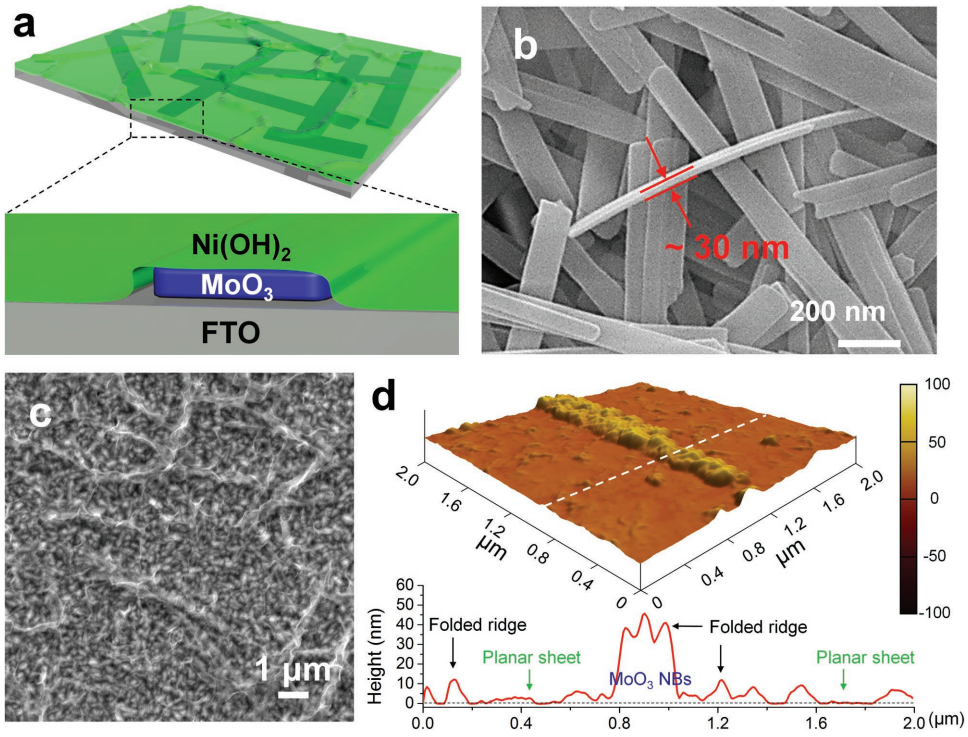

Figure 3. Growth of large-sized $Ni(OH)_2$ nanosheets/MoO_3 nanobelts hybrid film. a) Schematic illustrations of synthesis of $Ni(OH)_2/MoO_3$/FTO. b) SEM image of MoO_3 nanobelts. c) SEM image of $Ni(OH)_2/MoO_3$/FTO. d) The corresponding AFM 3D images of surface and height profiles along the white dash lines.

of a 2D heterolayered hybrid of $Ni(OH)_2/MoO_3$. Figure 3b and Figure S4 (Supporting Information) show the SEM and transmission electron microscopy (TEM) images of the MoO_3 nanobelt structures with an average width of 150 nm, thickness of 20–30 nm, and several micrometers in length. The interplanar lattice spacings are determined to be ≈0.40 and 0.37 nm, which correspond to the (100) and (001) planes of the α-MoO_3 phase.[29] Figure 3c and Figure S5 (Supporting Information) are the corresponding SEM images of 2D heterolayered hybrid of $Ni(OH)_2/MoO_3$. The underlying MoO_3 nanobelts are distinguishable after the growth of a thin layer of $Ni(OH)_2$ nanosheets. The belt-like structure with folded ridges shown in 3D AFM image (Figure 3d) is also observed which suggests $Ni(OH)_2$ outstretched growth over the MoO_3 nanobelts. It is noted that even after the MoO_3 nanobelts which are lack of −OH groups are sprayed on FTO substrate (Figure S6a, Supporting Information), the sparsely dispersed MoO_3 nanobelts did not change the inherent surface property of FTO. The MoO_3-nanobelts-coated FTO substrate is still largely covered by abundant hydrophilic −OH groups, as evident from the FTIR spectra (Figure S6b, Supporting Information). Hence, $Ni(OH)_2$ nanosheets show similar outstretched planar growth over the MoO_3 nanobelts that are sparsely deposited on the −OH rich FTO. Similar to $Ni(OH)_2$/FTO, the variations in AFM height profile that is measured along the white dash line display flat and ridge-like topography that corresponds to the planar nanosheets and the folded overlapping edges. Also, the width of 0.2 μm and thickness of 50 nm with folded ridge topography attributes to 2D $Ni(OH)_2$ growth over MoO_3 nanobelt. Notably, the $Ni(OH)_2$ film exhibits similar 2D anisotropic planar and outstretched growth over the flat MoO_3 nanobelts, implying the potential of integrating conformal multifunctional materials into an all-in-one platform. On the other hand, growth of 2D $Ni(OH)_2$ nanosheets on freestanding 2D MoO_3 nanobelts display the typical nonplanar 3D architecture of aggregated nanosheets that are assembled radially around the nanobelts (Figure S7, Supporting Information). The X-ray diffraction (XRD) spectra of $Ni(OH)_2$/FTO and $Ni(OH)_2/MoO_3$/FTO are shown in **Figure 4**a. Compared with the XRD spectrum of bare FTO glass, new peaks appeared at 12.6°, 33.2°, and 12.8°, 25.8°, 39.1° which can be attributed to (001), (110) crystal planes of α-$Ni(OH)_2$[24] (JCPDS card no. 22-0444) and (020), (040), (060) crystal planes of α-MoO_3[30] (JCPDS card no. 05-0508), respectively. The freestanding $Ni(OH)_2$ powder collected from the mother liquid can further confirm the α-$Ni(OH)_2$ crystalline phase (Figure S8, Supporting Information). The energy-dispersive X-ray spectroscopy (EDX) spectra of both $Ni(OH)_2$/FTO and $Ni(OH)_2/MoO_3$/FTO glass in Figure 4b show O and Ni peaks at 0.52, 0.85, and 7.47 keV, corresponding to the composition of $Ni(OH)_2$ nanosheets.[31] Mo peak can be seen at 2.30 keV in $Ni(OH)_2/MoO_3$/FTO glass, as the sprayed MoO_3 nanobelts layer.[29] The peaks at 3.06, 3.45, 3.67, 3.92, 4.14, and 4.36 are ascribed to Sn from the FTO glass substrate. X-ray photoelectron spectroscopy (XPS) analysis was also adopted to determine the chemical states of the $Ni(OH)_2$ nanosheets, particularly for Ni. The Ni 2p peak is shown in Figure 4c. The Ni $2p_{3/2}$ peak is located at 855.6 eV with a shakeup satellite peak at about 861.2 eV, and Ni $2p_{1/2}$ at 873.2 eV with a shakeup satellite peak at about 879.2 eV.[32] The gap between Ni $2p_{3/2}$ and Ni $2p_{1/2}$ is about 17.6 eV, which is in agreement with previous reports.[33]

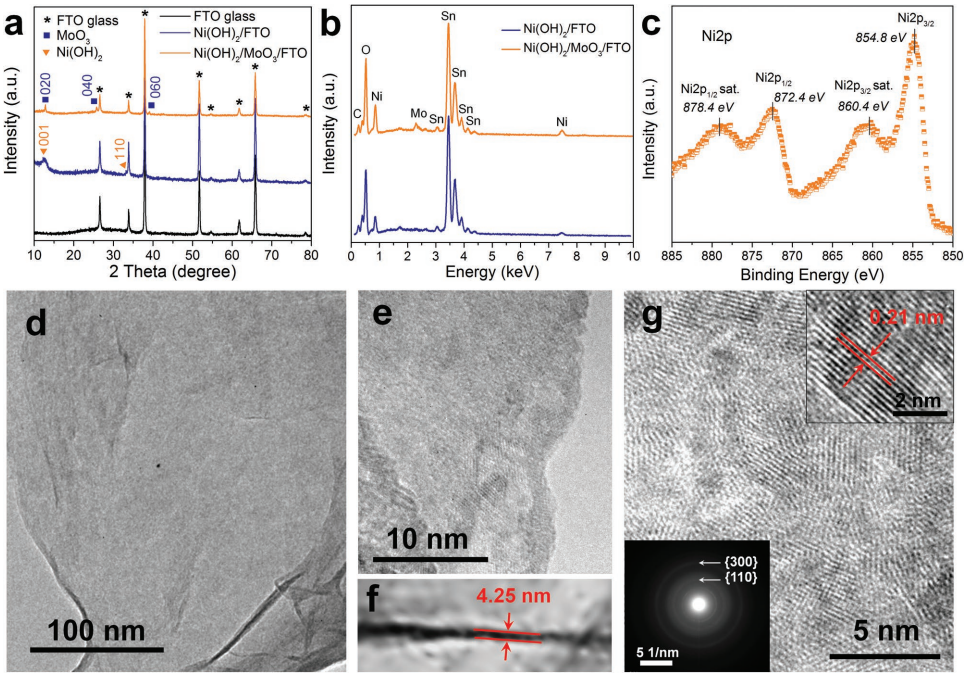

Figure 4. Characterization of the 2D nanosheets. a) XRD spectra of FTO, $Ni(OH)_2$/FTO, and $Ni(OH)_2/MoO_3$/FTO. b) High-resolution XPS spectra of Ni 2p of $Ni(OH)_2$/FTO. c) EDX spectra of $Ni(OH)_2$/FTO and $Ni(OH)_2/MoO_3$/FTO. d–f) TEM images of $Ni(OH)_2$ nanosheets. g) HRTEM images of the nanosheets, indicating that $Ni(OH)_2$ can easily be transformed into NiO under beam irradiation. Insets are large-magnification atomic structure (top) and the SAED pattern of $Ni(OH)_2$ nanosheets (bottom).

The TEM images (Figure 4d,e) show the $Ni(OH)_2$ nanosheets. The nearly transparent feature of the nanosheets indicates that they are fairly thin. The lighter contrast region depicts the flat planar $Ni(OH)_2$ film, while the curved darker lines present $Ni(OH)_2$ films, which are folded/crumpled into ridge-like structures. The thickness can be roughly estimated to be ≈4.25 nm from the folded or protuberant edge, composed of 5–8 layers of the $Ni(OH)_2$ nanosheets (Figure 4f).[34] Because the $Ni(OH)_2$ is sensitive to electron beam irradiation, lattice fringe of 0.21 nm in high-resolution TEM (HRTEM) images corresponds to (200) plane of NiO nanosheets which evolved from the $Ni(OH)_2$ nanosheets (Figure 4g).[35] The two marked selected area electron diffraction (SAED) rings correspond to the (110) and (300) planes of $Ni(OH)_2$ (Figure 4g, inset).[35,36]

The combined structural advantages of thin conformal layered film sanctions superior optical transparency, electrochemical activity, and structural stability. Correspondingly, proof-of-concept demonstration of electrochromism application is proposed as large homogeneous 2D materials are imperative for evaluation of electrochemical functionalities. Moreover, 2D nanomaterials, in particular the layered structures of $Ni(OH)_2$ possess unique strong lateral chemical bonding in planes contrasting with the weak van der Waals interaction between planes. The lamellar host framework consists of adequate interstitial spaces that facilitate high diffusion and insertion–extraction of guest species, grants an ideal and promising material for electrochemical devices. The samples were electrochemically characterized by cyclic voltammetry (CV) in 0.01 m NaOH electrolyte. No redox peaks were observed in the CV curve for bare FTO glass due to the absence of redox reactions. The CV curves of $Ni(OH)_2$/FTO glass in the potential window of 0–1.2 V (vs standard calomel electrode (SCE)) at various scan rates are shown in **Figure 5**a. A pair of redox peaks is observed in each curve and the intensities increase with scan rates. The cathodic peak shifted to the positive direction while the anodic peak shifted to the negative direction with the scan rate, suggesting the pseudocapacitive property of the material.[37] The current responses increase accordingly with the scan rates, while retaining the shapes of the CV curves. This suggests that the 2D hydrated layered $Ni(OH)_2$ nanosheets are beneficial for fast redox reactions. During the cathodic scan, the reduction of Ni^{3+} to Ni^{2+} leads to bleaching of the film. In the reverse anodic scan, the oxidation of Ni^{2+} to Ni^{3+} causes coloration of the film. The OH^- intercalation–deintercalation and electron transfer can be attributed to the electrochemical reactions of $Ni(OH)_2$ as follows[38–40]

$$[Ni(OH)_2 + OH^-]_{bleached} \leftrightarrow [NiOOH + H_2O + e^-]_{colored} \quad (1)$$

The electrochromic effect measured in the neutral electrolyte solution (0.5 m Na_2SO_4) is shown in Figure 5b, where the coated glass was repeatedly switched between the bleached and colored states at different voltage biases, and the corresponding change in relative transmittance over time was recorded. The relative transmittances of the coating in the bleached and colored states were observed to be consistent. It can be seen that over the five switching cycles, the $Ni(OH)_2/MoO_3$/FTO glass consistently exhibited a relative transmittance level of 18.8%, 60.6%, and 82.2% at 2.5, 2.0, and 1.5 V, respectively, in its colored state. The transmittance spectra of the $Ni(OH)_2/MoO_3$/FTO glass recorded at +2.5 V were shown in the Figure 5c. It is noted that the

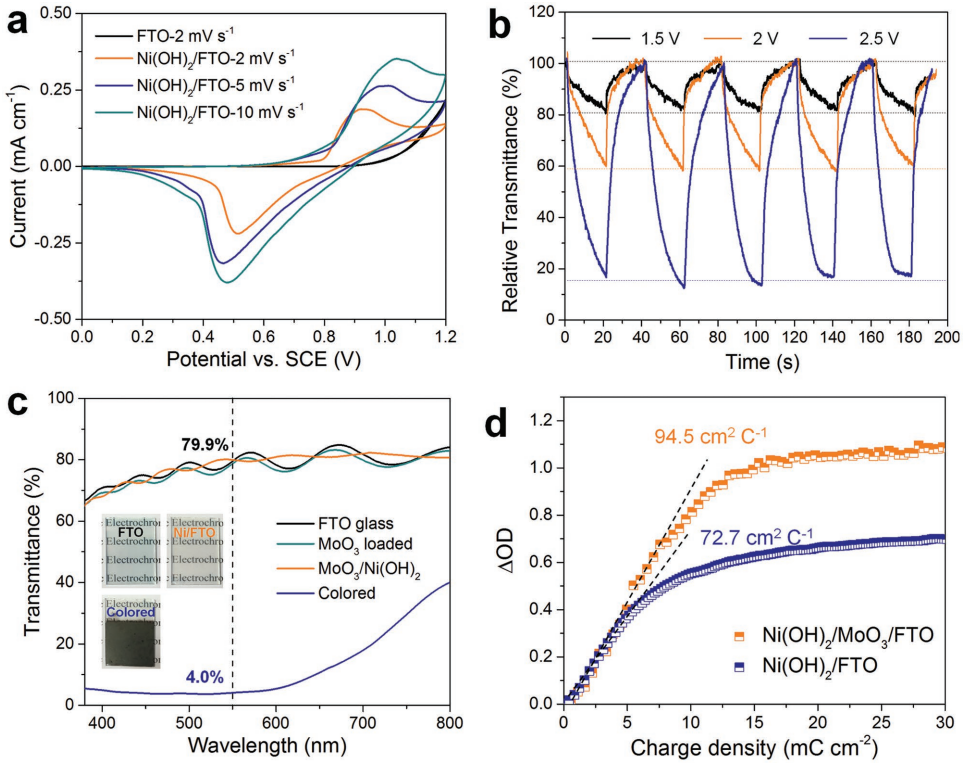

Figure 5. Supercapacitive electrochromics of $Ni(OH)_2$ nanosheets on FTO glass. a) Cyclic voltammograms (CV) of FTO and $Ni(OH)_2$/FTO glass in 0.01 m NaOH at various scan rates. b) Transmittance spectra of $Ni(OH)_2$/FTO over consecutive cycles of bleaching and coloration with various voltage biases in 0.5 m Na_2SO_4 at 550 nm. c) Transmittance spectra of $Ni(OH)_2/MoO_3$/FTO in one cycle of bleaching and coloration. Insets are the corresponding photos of $Ni(OH)_2/MoO_3$/FTO at different conditions. d) Optical density versus charge density of $Ni(OH)_2/MoO_3$/FTO and $Ni(OH)_2$/FTO recorded at 550 nm.

transmittance of the bleached samples is almost the same as bare FTO glass, indicating the transparency of the thin $Ni(OH)_2$ layer. Moreover, the good coloration performance is also determined by applying +2.5 V voltage on $Ni(OH)_2$/FTO glass. The transmittance of 4.0% in colored state is attained at 550 nm, while that of bleached state is 79.9% at the same wavelength. The corresponding digital photographs of bleached and colored states of the $Ni(OH)_2$/FTO glass are shown in Figure 5c insets. The corresponding coloration efficiencies (CE) of $Ni(OH)_2/MoO_3$/FTO and $Ni(OH)_2$/FTO are calculated to be 94.5 and 72.7 $cm^2\ C^{-1}$ (Figure 5d), respectively, which are higher than the reported CE of $Ni(OH)_2$ or NiO in many papers.[41–44]

In light of the compelling needs and great potential of 2D nanosheets for flexible technologies, a range of flexible traits from bendable, rollable to foldable thin $Ni(OH)_2$ film on various supports are demonstrated (**Figure 6**a–d). Figure 6e,f shows the typical film morphology of direct growth of homogeneous $Ni(OH)_2$ nanosheets on ITO–PET and paper, respectively. The slight tinge of color change over a large area on paper and ITO–PET before and after the growth of $Ni(OH)_2$ planar nanosheets suggests the possibility of fabricating scalable thin, flexible electronics on such supports (Figure S10, Supporting Information). Moreover, Figure S11 (Supporting Information) shows the surfaces of ITO–PET and paper after respective rolling and folding, which remains intact or undelaminated film. The characterization of EDX and XRD is carried out to further confirm the successful growth of α-$Ni(OH)_2$ as shown in Figure 6g,h. The electrochromic performance of $Ni(OH)_2$/ITO–PET is investigated and transmittance spectra are presented in Figure 6i. The $Ni(OH)_2$/ITO–PET film shows a slight decrease in transmittance of bleached state, while a remarkable reduction to that of colored state, at 2.5 V with the transmittance in the wavelength of 550 nm dropping to about 29.7%. In comparison to $Ni(OH)_2$/FTO glass, the contrast between bleached and colored states of $Ni(OH)_2$/ITO–PET is lower, which is attributed to the higher electrical resistance of ITO–PET. To further validate the mechanical stability of the flexible sample, the $Ni(OH)_2$/ITO–PET was mechanically bent from 156° to 75° for 1000 times (Figure 6j). From the corresponding transmittance spectra (Figure 6k), it is can be seen that the electrochromic property at 2 V is fairly stable with reduced transmission contrast of 3.5% as compared with those before bending. The electrochemical performance of $Ni(OH)_2$/ITO–PET at bleached and colored states operated at voltage bias at 550 nm was observed to be rather consistent over the switching cycles (Figure S12, Supporting Information). However, excessive flexing beyond 75° will lead to uniaxial cracking of the ITO on PET (Figure S13a,b, Supporting Information) since ITO is known to be fragile and brittle.[45,46] Evidently, SEM image shows no delamination or peeling of the active $Ni(OH)_2$ layer from the ITO–PET surface, even at the edges of parallel crack lines that are marked with arrows

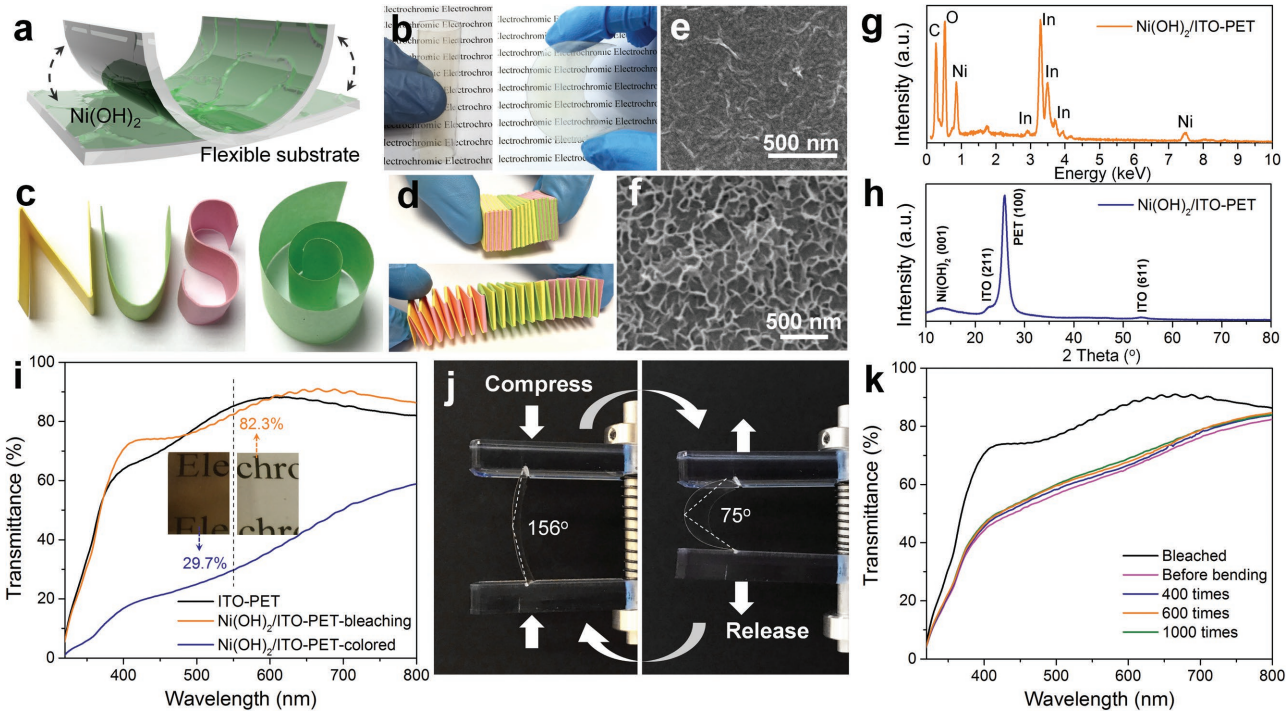

Figure 6. $Ni(OH)_2$ nanosheets on flexible substrates and flexible electrochromism. a) Schematic structure. Photographs of the b) bent $Ni(OH)_2$/ITO–PET, c) rolled $Ni(OH)_2$/paper, and d) folded $Ni(OH)_2$/paper. SEM images of flexible e) $Ni(OH)_2$/ITO–PET and f) $Ni(OH)_2$/paper. g) EDX and h) XRD spectra of $Ni(OH)_2$/ITO–PET. i) Transmittance spectra of $Ni(OH)_2$/ITO–PET in one bleaching and coloration cycle. Insets show the corresponding photos of $Ni(OH)_2$/ITO–PET under different conditions. j) Photographs of mechanical bending of $Ni(OH)_2$/ITO–PET. k) Transmittance spectra of $Ni(OH)_2$/ITO–PET before and after bending 1000 times.

(Figure S13c, Supporting Information). It can be deduced from the bending experiments that the cracking of the ITO has been viewed as the limiting factor instead of $Ni(OH)_2$ adhesion on the substrate. These observations unambiguously suggest strong bonding of electrochromic active layer to the underlying substrate owing to direct conformal planar growth of $Ni(OH)_2$ nanosheets onto support which maximizes the interfacial contact.

Direct 2D anisotropic growth of nanostructures which are homogeneous and scalable has demonstrated to be an effective and straightforward way to readily fulfill transparent flexible technologies requirements. 2D planar growth of thin $Ni(OH)_2$ nanosheets is realized on both rigid and soft supports through a direct adsorption-oriented attachment growth mechanism and the intrinsic lamellar structure formation. Moreover, the planar layered growth of $Ni(OH)_2$ nanosheets has shown the ability to integrate with other 2D material, i.e., MoO_3 nanobelts, which establishes an easy pathway to the construction of heterostructures for hybrid functionalities. To the end, proof-of-concept electrochromism testify the optical and electrochemical properties of the as-prepared 2D materials with wide optical modulation of ≈52%–76%, high coloration efficiency of 72.7–94.5 $cm^2\ C^{-1}$, and good cyclic stability and flexibility attributes. Such direct growth approach is well-suited for diversified fundamental studies and proof-of-concept demonstrations where thin homogeneous materials are desired, i.e., catalysis, sensing, chromism, electronic devices, such as field-effect transistors and logic circuits, etc.

Supporting Information

Supporting Information is available from the Wiley Online Library or from the author.

Acknowledgements

This work was supported by the National Research Foundation Singapore, Ministry of National Development, R-263-000-C22-277.

[1] S. Z. Butler, S. M. Hollen, L. Cao, Y. Cui, J. A. Gupta, H. R. Gutiérrez, T. F. Heinz, S. S. Hong, J. Huang, A. F. Ismach, E. Johnston-Halperin, M. K. Vladimir, V. Plashnitsa, R. D. Robinson, R. S. Ruoff, S. Salahuddin, J. Shan, L. Shi, M. G. Spencer, M. Terrones, W. Windl, J. E. Goldberger, *ACS Nano* **2013**, *7*, 2898.
[2] M. Chhowalla, H. S. Shin, G. Eda, L. J. Li, K. P. Loh, H. Zhang, *Nat. Chem.* **2013**, *5*, 263.
[3] F. Saleem, Z. Zhang, B. Xu, X. Xu, P. He, X. Wang, *J. Am. Chem. Soc.* **2013**, *135*, 18304.
[4] L. Yu, Y. H. Lee, X. Ling, E. J. G. Santos, Y. C. Shin, Y. Lin, M. Dubey, E. Ka xiras, J. Kong, H. Wang, T. Palacios, *Nano Lett.* **2014**, *14*, 3055.
[5] S. Wu, R. Xu, M. Lu, R. Ge, J. Iocozzia, C. Han, B. Jiang, Z. Lin, *Adv. Energy Mater.* **2015**, *5*, 1500400.
[6] S. J. Kim, K. Choi, B. Lee, Y. Kim, B. H. Hong, *Annu. Rev. Mater. Res.* **2015**, *45*, 63.

[7] X. Zhang, Y. Lai, Y. Zeng, K. Zhang, Z. Lin, *J. Mater. Chem. A* **2015**, *3*, 12761.
[8] M. Zeng, L. Wang, J. Liu, T. Zhang, H. Xue, Y. Xiao, Z. Qin, L. Fu, *J. Am. Chem. Soc.* **2016**, *138*, 7812.
[9] Y. Wang, Z. Ni, Q. Liu, R. Quhe, J. Zheng, M. Ye, D. Yu, J. Shi, J. Yang, J. Li, J. Lu, *Adv. Funct. Mater.* **2015**, *25*, 68.
[10] X. Wang, F. Xia, *Nat. Mater.* **2015**, *14*, 264.
[11] J. H. Yu, H. R. Lee, S. S. Hong, D. Kong, H. W. Lee, H. Wang, F. Xiong, S. Wang, Y. Cui, *Nano Lett.* **2015**, *15*, 1031.
[12] X. Yuan, L. Tang, S. Liu, P. Wang, Z. Chen, C. Zhang, Y. Liu, W. Wang, Y. Zou, C. Liu, N. Guo, J. Zou, P. Zhou, W. Hu, F. Xiu, *Nano Lett.* **2015**, *15*, 3571.
[13] M. He, D. Zheng, M. Wang, C. Lin, Z. Lin, *J. Mater. Chem. A* **2014**, *2*, 5994.
[14] A. Castellanos-Gomez, M. Buscema, R. Molenaar, V. Singh, L. Janssen, H. S. van der Zant, G. A. Steele, *2D Mater.* **2014**, *1*, 011002.
[15] L. Niu, J. N. Coleman, H. Zhang, H. Shin, M. Chhowalla, Z. Zheng, *Small* **2016**, *12*, 272.
[16] M. He, J. Jung, F. Qiu, Z. Lin, *J. Mater. Chem.* **2012**, *22*, 24254.
[17] J. Kang, J. Li, S. S. Li, J. B. Xia, L. W. Wang, *Nano Lett.* **2013**, *13*, 5485.
[18] T. Georgiou, R. Jalil, B. D. Belle, L. Britnell, R. V. Gorbachev, S. V. Morozov, Y. J. Kim, A. Gholinia, S. J. Haigh, O. Makarovsky, L. Eaves, L. A. Ponomarenko, A. K. Geim, K. S. Novoselov, A. Mishchenko, *Nat. Nanotechnol.* **2013**, *8*, 100.
[19] M. Y. Li, C. H. Chen, Y. Shi, L. J. Li, *Mater. Today* **2016**, *19*, 322.
[20] J. Wang, L. Zhang, L. Yu, Z. Jiao, H. Xie, X. W. Lou, X. W. Sun, *Nat. Commun.* **2014**, *5*, 4921.
[21] J. W. Liu, J. Zheng, J. L. Wang, J. Xu, H. H. Li, S. H. Yu, *Nano Lett.* **2013**, *13*, 3589.
[22] L. Liang, J. Zhang, Y. Zhou, J. Xie, X. Zhang, M. Guan, B. Pan, Y. Xie, *Sci. Rep.* **2013**, *3*, 1936.
[23] X. Liu, A. Zhou, Y. Dou, T. Pan, M. Shao, J. Han, M. Wei, *Nanoscale* **2015**, *7*, 17088.
[24] R. Li, Z. Hu, X. Shao, P. Cheng, S. Li, W. Yu, W. Lin, D. Yuan, *Sci. Rep.* **2016**, *6*, 18737.
[25] Z. Xu, J. Yu, G. Liu, B. Cheng, P. Zhou, X. Li, *Dalton Trans.* **2013**, *42*, 10190.
[26] H. Yan, J. Bai, J. Wang, X. Zhang, B. Wang, Q. Liu, L. Liu, *CrystEngComm* **2013**, *15*, 10007.
[27] J. Yan, Z. Fan, W. Sun, G. Ning, T. Wei, Q. Zhang, R. Zhang, L. Zhi, F. Wei, *Adv. Funct. Mater.* **2012**, *22*, 2632.
[28] Z. Li, J. Han, L. Fan, R. Guo, *Colloid Polym. Sci.* **2016**, *294*, 681.
[29] D. Chen, M. Liu, L. Yin, T. Li, Z. Yang, X. Li, B. Fan, H. Wang, R. Zhang, Z. Li, H. Xu, H. Lu, D. Yang, J. Sun, L. Gao, *J. Mater. Chem.* **2011**, *21*, 9332.
[30] Z. Wang, S. Madhavi, X. W. Lou, *J. Phys. Chem. C* **2012**, *116*, 12508.
[31] K. Zhou, W. Zhou, L. Yang, J. Lu, S. Cheng, W. Mai, Z. Tang, L. Li, S. Chen, *Adv. Funct. Mater.* **2015**, *25*, 7530.
[32] I. Chang, T. T. Chen, M. H. Yang, H. T. Chiu, C. Y. Lee, *J. Mater. Chem. A* **2014**, *2*, 10370.
[33] L. Zhang, Q. Ding, Y. Huang, H. Gu, Y. E. Miao, T. Liu, *ACS Appl. Mater. Interfaces* **2015**, *7*, 22669.
[34] Y. Zhu, C. Cao, S. Tao, W. Chu, Z. Wu, Y. Li, *Sci. Rep.* **2014**, *6*, 5787.
[35] H. Fan, X. Huang, L. Shang, Y. Cao, Y. Zhao, L. Z. Wu, T. Zhang, *Angew. Chem., Int. Ed.* **2016**, *55*, 2167.
[36] W. Zhou, X. Cao, Z. Zeng, W. Shi, Y. Zhu, Q. Yan, H. Liu, J. Wang, H. Zhang, *Energy Environ. Sci.* **2013**, *6*, 2216.
[37] T. Zhu, J. Wang, G. W. Ho, *Nano Energy* **2015**, *18*, 273.
[38] W. L. Ong, S. W. L. Ng, C. Zhang, M. Hong, G. W. Ho, *J. Mater. Chem. A* **2016**, *4*, 13307.
[39] F. Grote, Z. Y. Yu, J. L. Wang, S. H. Yu, Y. Lei, *Small* **2015**, *11*, 4666.
[40] T. Gao, B. P. Jelle, *J. Phys. Chem. C* **2013**, *117*, 17294.
[41] L. Guo, Y. Ren, J. Liu, S. Y. Chiam, W. K. Chim, *Small* **2014**, *10*, 2611.
[42] X. H. Xia, J. P. Tu, J. Zhang, X. L. Wang, W. K. Zhang, H. Huang, *Sol. Energy Mater. Sol. Cells* **2008**, *92*, 628.
[43] C. C. Streinz, A. P. Hartman, S. Motupally, J. W. Weidner, *J. Electrochem. Soc.* **1995**, *142*, 1084.
[44] J. Y. Ji, L. L. Zhang, H. X. Ji, Y. Li, X. Zhao, X. Bai, X. B. Fan, F. B. Zhang, R. S. Ruoff, *ACS Nano* **2013**, *7*, 6237.
[45] H. K. Lin, S. M. Chiu, T. P. Cho, J. C. Huang, *Mater. Lett.* **2013**, *113*, 182.
[46] S. I. Na, S. S. Kim, J. Jo, D. Y. Kim, *Adv. Mater.* **2008**, *20*, 4061.

Received: January 8, 2017
Revised: February 21, 2017
Published online: May 2, 2017

